Cell. Mol. Life Sci. (2016) 73:185–200
DOI 10.1007/s00018-015-1987-y

Cellular and Molecular Life Sciences

ORIGINAL ARTICLE

Molecular basis of claudin-17 anion selectivity

Marcel P. Conrad[1] · Jörg Piontek[1] · Dorothee Günzel[1] · Michael Fromm[1] · Susanne M. Krug[1]

Received: 20 April 2015 / Revised: 23 June 2015 / Accepted: 9 July 2015 / Published online: 21 July 2015

Abstract Claudin-17 is a paracellular channel-forming tight junction protein. Unlike the cation channels claudin-2 and -15, claudin-17 forms a distinct anion-selective channel. Aim of this study was to determine the molecular basis of channel formation and charge selectivity of this protein. To achieve this, residues located in the extracellular loops (ECL) 1 and 2 of claudin-17 were substituted, preferably those whose charges differed in claudin-17 and in claudin-2 or -15. The respective mutants were stably expressed in MDCK C7 cells and their ability to form charge-selective channels was analyzed by measuring ion permeabilities and transepithelial electrical resistance. The functional data were combined with homology modeling of the claudin-17 protomer using the structure of claudin-15 as template. In ECL1, K65, R31, E48, and E44 were found to be stronger involved in Cldn17 channel function than the clustered R45, R56, R59, and R61. For K65, not only charge but also stereochemical properties were crucial for formation of the anion-selective channel. In ECL2, both Y149 and H154 were found to contribute to constitution of the anion channel in a distinct manner. In conclusion, we provide insight into the molecular mechanism of the formation of charge- and size-selective paracellular ion channels. In detail, we propose a hydrophilic furrow in the claudin-17 protomer spanning from a gap between the ends of TM2 and TM3 along R31, E48, and Y67 to a gap between K65 and S68 lining the anion channel.

Keywords Tight junctions · Claudin-17 · Paracellular permeability · Charge selectivity

Abbreviations

TJ	Tight junction
Cldn	Claudin
Occl	Occludin
SEM	Standard error of the mean
MDCK	Madin-Darby Canine Kidney
TER	Transepithelial resistance
wt	Wildtype
vec	Vector control
TM	Transmembrane segment
ECL1 and -2	Extracellular loop 1 and 2, equivalent to extracellular segment 1 and 2

Introduction

Tight junctions (TJ) are structures formed by multi-protein complexes that on one hand tighten the paracellular cleft of epi- and endothelia against unwanted passage of solutes, but on the other hand also allow and regulate tissue-specific paracellular permeation. These selectivity properties are fundamentally based on the presence or absence of distinct members of the transmembrane protein family of claudins. Claudins exhibit a tetraspan topology [as do TJ-associated MARVEL proteins (TAMPs)] with two extracellular loops (ECLs), a larger first extracellular loop (ECL1, also called extracellular segment 1) and a smaller second one (ECL2,

M. P. Conrad and J. Piontek contributed equally to the study.

Electronic supplementary material The online version of this article (doi:10.1007/s00018-015-1987-y) contains supplementary material, which is available to authorized users.

✉ Susanne M. Krug
susanne.m.krug@charite.de

[1] Institute of Clinical Physiology, Charité, Universitätsmedizin Berlin, Campus Benjamin Franklin, Hindenburgdamm 30, 12203 Berlin, Germany

also called extracellular segment 2). Generally, ECL1 is considered to be responsible for the charge and size selectivity of the claudins [1–4]. There are currently 27 claudins known in mammals [5] and most of the so far characterized claudins possess sealing effects on the TJ.

However, some claudins have been shown to form paracellular channels selective in charge and size [6]. While Cldn2 [7], Cldn10b [8, 9], and Cldn15 [10] are selective for cations, Cldn10a [8, 9] and Cldn17 [11] act as anion-selective channel-forming claudins. Additionally, Cldn2 has been shown to be responsible for paracellular water permeability [12].

These different properties of claudins, though sharing high sequence similarities, early raised interest in the characterization of amino acid residues and/or motifs determining pore and selectivity formation. Using site-directed mutagenesis, a number of amino acid residues in ECL1 were identified to be essential for proper claudin function. Cldn2 in this context has been analyzed best so far. Yu and coworkers used cysteine-scanning mutagenesis as well as Brownian dynamics simulations to create a detailed preliminary model of the Cldn2 channel architecture [13, 14]. In this model, position 65 was highlighted as a key determinant of channel function.

For other claudins, less detailed information is available. However, the ability of Cldn10a to form a preferentially anion-selective channel depends mainly on the positions R32 and R59 [8]. In Cldn5, a sealing TJ protein of the blood–brain barrier, the cysteine residue at position 64, which, together with C54, is conserved in all claudins, is essential to maintain barrier properties [15].

More recently, the second extracellular loop came into focus as a determinant of barrier function, as Piehl et al. demonstrated that substitution of amino acid residues in the ECL2 of Cldn5 at positions R145, Y148, Y158, E159 leads to decreased transepithelial resistance (TER) and impaired sealing function for small ions and larger molecules compared to that in wildtype Cldn5 [16].

This and similar functional data were used to generate first models of the ECL2 of classic claudins [17, 18]. However, a more detailed structural understanding of barrier and channel formation was limited due to the lack of 3D structure information for claudins. Recently, however, the first claudin crystal structures have been published for Cldn15 and Cldn19 [19, 20]. This now allows more detailed homology modeling of other classic claudins and investigation of the molecular mechanisms responsible for channel formation.

In the present study, we performed a detailed functional analysis of Cldn17, introducing charge-reversing or charge-neutralizing mutations and analyzing their impact on anion permeability. The resulting effects were combined with homology modeling of the structure of the human Cldn17 protomer (structural unit of the TJ strands), using the published crystal structure of mouse Cldn15 as template. It was noted that besides K65 [11] further residues in ECL1 and ECL2 are involved in the paracellular channel formation and charge selectivity of Cldn17. Taken together, this study provides, for the first time in an anion channel-forming claudin, molecular insights into paracellular ion channel formation which may be relevant for and also transferable to other channel-forming claudins.

Materials and methods

Cell culture

Madin-Darby canine kidney (MDCK) C7 and HEK293 cells were maintained in Minimum Essential Medium (MEM, Sigma-Aldrich), supplemented with 10 % fetal bovine serum (FBS, Sigma-Aldrich), 100 U/ml penicillin, and 100 mg/ml streptomycin (PAA, Pasching, Austria). MDCK C7 cells stably transfected with wildtype Cldn17 were maintained as described before [11].

Transfection and site-directed mutagenesis

MDCK C7 cells were stably transfected with p3 × FLAG-CMV-10 containing human - or mutated Cldn17 cDNA by employing Lipofectamine Plus according to the manufacturer's instruction (Life technologies, Darmstadt, Germany). Cell clones resistant to G418 (Biochrome, Berlin, Germany) were screened for FLAG expression by Western blotting and TJ localization by immunofluorescence microscopy.

Mutant Cldn17 cDNA was generated by PCR amplification applying the primers listed in Table 1. Point mutations were verified by sequencing. Human wildtype Cldn17 and Cldn17 mutants were cloned using different sites within the vector's multiple cloning site. Therefore, linker sequences between FLAG-Tag and Cldn17 start codon differ in length by 12 bp, resulting in different protein masses, which can be seen in immunoblots as a slight shift.

Immunofluorescence microscopy

Cells were grown on glass slides for 5 days and fixed with methanol for 10 min at −20 °C. For permeabilization, cells were treated for 7 min with 0.5 % Triton X-100 in phosphate-buffered saline (PBS) containing Ca^{2+} and Mg^{2+}. Additionally, cells were incubated for 15 min with blocking solution (5 % goat serum in PBS) to minimize unspecific antibody binding. Antibodies were diluted in blocking solution, mouse anti FLAG-M2 (Sigma Aldrich,

Table 1 Primers used for generation of the respective mutations of human Cldn17

Name	Mutation	Sequence (5′–3′)
Flanking forw	–	CCAAGCTTCGTATGGCATTTTATCCCTTGCAAATTG
Flanking rev	–	CGCGGATCCTTAGACATAACTGGTGGAGGTCTT
R31E forw	R31E	CCTTCTGCCTCAGTGGGAAGTATCAGCTTT
R31E rev	R31E	AAAGCTGATACTTCCCACTGAGGCAGAAGG
E44A forw	E44A	AACATTATTGTCTTTGCGAGGCTCTGGGAAG
E44A rev	E44A	CTTCCCAGAGCCTCGCAAAGACAATAATGTT
R45A forw	R45A	CATTATTGTCTTTGAGGCGCTCTGGGAAGG
R45A rev	R45A	CCTTCCCAGAGCGCCTCAAAGACAATAATG
E48K forw	E48K	GCTCTGGAAAGGGCTCTGGATGAATTGCAT
E48K rev	E48K	GAGCCCTTTCCAGAGCCTCTCAAAGACAATAAT
E48Q forw	E48Q	TCTTTGAGAGGCTCTGGCAAGGGCTCTGAA
E48Q rev	E48Q	GAGCCCTTGCCAGAGCCTCTCAAAGACAATAATG
R56A forw	R56A	GAATTGCATCGCACAAGCCAGGGTCCGGTTG
R56A rev	R56A	CAACCGCGACCCTGGCTTGTGCGATGCAATTC
R56T forw	R56T	GAATTGCATCACACAAGCCAGGGTCCGGTTG
R56T rev	R56T	CAACCGCGACCCTGGCTTGTGTGATGCAATTC
R59A forw	R59A	CATCCGACAAGCCGCGGTCCGGTTGCAATG
R59A rev	R59A	CATTGCAACCGGACCGCGGCTTGTCGGATG
R61A forw	R61A	GACAAGCCAGGGTCGCGTTGCAATGC
R61A rev	R61A	GCATTGCAACGCGACCCTGGCTTGTC
K65A forw	K65A	AGGGTCCGGTTGCAATGCGCGTTCTATAGC
K65A rev	K65A	CTATAGAACGCGCATTGCAACCGGACCCTG
K65E forw	K65E	AGGGTCCGGTTGCAATGCGAGTTCTATAGC
K65E rev	K65E	CTATAGAACTCGCATTGCAACCGGACCCTG
K65R forw	K65R	AGGGTCCGGTTGCAATGCAGGTTCTATAGC
K65R rev	K65R	CTATAGAACCTGCATTGCAACCGGACCCTG
Y149A forw	Y149A	CATCAGAGATTTCGCCAACCCAGCCATC
Y149A rev	Y149A	GATGGCTGGGTTGGCGAAATCTCTGATG
H154A forw	H154A	CAACCCAGCCATCGCCATAGGTCAGAAAC
H154A rev	H154A	GTTTCTGACCTATGGCGATGGCTGGGTTG
S68E forw	S68E	AGTTCTATGAGTCCTTGTTGGCT
S68E rev	S68E	AGCCAACAAGGACTCATAGAACT

1:600), and rabbit anti-occludin (Invitrogen, 1:200), and applied for at least 60 min. After washing, cells were exposed to secondary antibodies (DyLight488 goat anti rabbit 1:500 (Jackson, Suffolk, UK), AlexaFluor 594 goat anti mouse (Invitrogen) 1:500) and DAPI (1:1000) for 60 min and subsequently mounted on microscope slides using ProTag MountFluor (Biocyc, Luckenwalde, Germany). Images were obtained with a confocal laser scanning microscope (LSM Meta 510, Zeiss, Jena, Germany).

Western blotting

Cells were scraped from culture dishes after washing with PBS and homogenized in lysis buffer (20 mM Tris, 5 mM $MgCl_2$, 1 mM EDTA, 0.3 mM EGTA) containing a protease inhibitor mix (Roche, Mannheim, Germany). Membrane fractions were obtained by passing through a 26-G 1/2 needle, followed by a centrifugation at $200\times g$ for 5 min and a subsequent centrifugation of the remaining supernatant at $43{,}000\times g$ for 30 min. Membrane protein was enriched in the pellet and resuspended in lysis buffer. Protein quantification was performed using BCA protein assay reagent (Pierce, Rockford, IL, USA) and a plate reader (Tecan, Grödig, Austria). For analysis, protein samples were prepared with Laemmli buffer and denatured at 95 °C for 5 min before loading. After separation on SDS-PAGE (12.5 % for Cldn analysis and 7.8 % for occludin), proteins were blotted on a PVDF membrane (Perkin Elmer, Boston, MA, USA) and proteins of interest

were detected using FLAG-M2 antibody and a luminescence imaging system (Fusion FX-7, Vilber Lourmat).

Dilution potential measurements

For dilution potential measurements, cells were grown on filter supports (Millicell®-HA culture plate inserts, area: 0.6 cm^2, pore size: 0.45 µm; Millipore, Ireland) to confluence and mounted into Ussing chambers. Resistance of bathing solution was measured prior to each experiment and subtracted. Ussing chambers and water-jacketed gas lifts were kept at 37 °C and filled with 10 ml modified Ringer's solution [in mM: NaCl 140; KCl 5.4; $CaCl_2$ 1.2; $MgCl_2$ 1; HEPES 10; D(+)-glucose 10] and pH was adjusted to 7.4 with NaOH. The solution was equilibrated with 100 % O_2.

NaCl dilution potentials were measured by switching one hemichamber to a solution containing a reduced concentration of NaCl and all other components identical to standard Ringer's solution. Osmolality was balanced by mannitol [in mM: NaCl 70; mannitol 140; KCl 5.4; $CaCl_2$ 1.2; $MgCl_2$ 1; HEPES 10; D(+)-glucose 10]. For biionic potentials of selected monovalent anions, the solution in one hemichamber was changed to one in which 50 % of the NaCl was replaced isoosmotically by the respective sodium anion salt [NaCl 70; $NaNO_3$/Na-pyruvate/NaSCN 70; KCl 5.4; $CaCl_2$ 1.2; $MgCl_2$ 1; HEPES 10; D(+)-glucose 10]. Permeabilities were calculated employing the Goldman–Hodgkin–Katz equation.

Fluorescein flux measurements

Measurements of unidirectional fluxes from apical to basolateral side were performed in Ussing chambers under short circuit conditions. Ussing chambers were filled with 10 ml standard Ringer's solution [in mM: NaCl 119; $NaHCO_3$ 21; KCl 5.4; $MgSO_4$ 1; $CaCl_2$ 1.2; HEPES 3; D(+)-glucose 10] per side, and equilibrated with 95 % O_2 and 5 % CO_2. 10 µl of fluorescein (100 mM) was added apically, and basolateral samples (300 µl) were replaced by fresh Ringer's solution 0, 30, 60, 90, 120, and 150 min after addition. Samples were analyzed with a fluorometer (Spectramax Gemini, Molecular devices) at 520 nm and used for calculation of fluxes and permeability.

Live cell imaging for trans-interaction analysis

For trans-interaction analysis, HEK293 cells, a cell line devoid of TJs, were grown on poly-L-lysine-treated Labteks (Thermo Fisher Scientific, Rochester, NY, USA) to 80 % confluence and transfected with N-terminally CFP-tagged Cldn17wt, $Cldn17_{Y149A}$, or $Cldn17_{H154A}$. 24 h after transfection, cells were washed and incubated in HEPES-buffered Ringer's solution. For marking of cell membranes, cells were incubated with trypan blue (Chroma, Stuttgart, Germany) and the enrichment of claudins at contacts between claudin-expressing cells as a measure of trans-interaction was analyzed using a confocal laser scanning microscope (LSM Meta 510, Zeiss, Jena, Germany) as described previously [17].

Freeze-fracture electron microscopy

Cells grown on permeable supports were fixed with phosphate-buffered glutaraldehyde (2 %) and subsequently incubated in 10 % (v/v), then in 30 % (v/v) glycerol, and finally frozen in liquid nitrogen-cooled Freon 22. Cells were fractured at −100 °C and shadowed with platinum and carbon in a vacuum evaporator (Denton DV-502). Replicas were bleached with sodium hypochloride, picked up on grids (Ted Pella Inc.), and analyzed with a video-equipped Zeiss 902A electron microscope (Carl Zeiss AG; Olympus iTEM Veleta). Morphometric analysis was performed at a final magnification of 51,000× as described before [11].

Structural modeling of Cldn17

First homology models were generated using swissmodel (http://swissmodel.expasy.org/; [21–23]). The crystal structure of murine Cldn15 ([19]; PDB ID 4P79) was used as template. Model quality was estimated employing the QMEAN server (http://swissmodel.expasy.org/qmean/cgi/index.cgi; [24]). For the Cldn17 model based on PDB 4P79, an average local per-residue error of 2.8 ± 1.9 Å was obtained. In addition, I-TASSER (http://zhanglab.ccmb.med.umich.edu/I-TASSER/) was used and resulted in similar models. Using PyMOL (version 1.5.0.4 Schrödinger, LLC), the residues mutated in this study were mapped on the model. For generation of a basic schema of the potential architecture of the polymeric TJ strand, the double row model of Cldn15 TJ strands [25] was built and modified by manual positioning of the protomers using PyMOL. Electrostatic potentials were calculated and displayed as potentials on the solvent-accessible surface using the Adaptive Poisson-Boltzmann Solver (APBS, MG Lerner and HA Carlson. APBS plugin for PyMOL, 2006, University of Michigan, Ann Arbor; units *kT/e*). For APBS, a Cldn15 model based on PDB 4P79 was obtained from swissmodel (model_id: 82d2e7bffef9d f54039dd9d1e05b7b48_UP000055_1EXPDTA).

Statistics

Data represent mean values ± standard error of the mean (SEM). Statistical analysis was performed using Student's

t test and Bonferroni–Holm correction for multiple testing. Values $p < 0.05$ were considered significant.

Results

Sequence analysis of Cldn17 revealed four charged residues within the ECL1 that were different from the respective positions in two cation-selective claudins, Cldn2 or Cldn15 (Fig. 1a for ECL1, Fig. 4a for ECL2). The respective charges were conserved between 28 available orthologous Cldn17 sequences (Fig. S1). Thus, investigation of the impact on ion selectivity focused on these positions. Furthermore, the species comparison of Cldn17 showed three arginines within ECL1 of human Cldn17 to be less conserved, e.g., absent in murine Cldn17, suggesting that these positions have less influence (Fig. 3a).

The respective positions were mutated to charge-reversing or neutral amino acids (Table 2). Empty vector-transfected MDCK C7 cells served as negative controls.

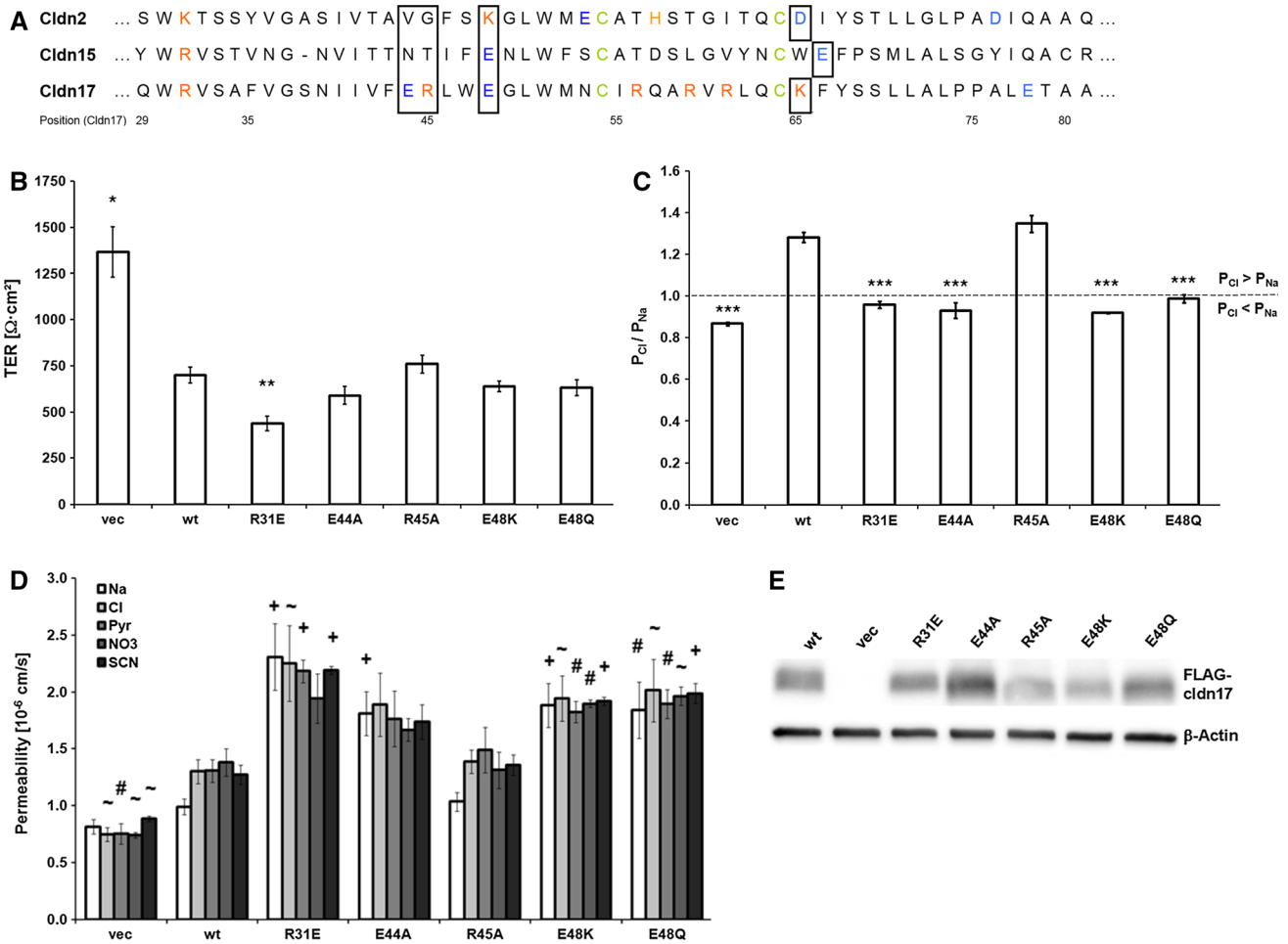

Fig. 1 Mutation of amino acid residues within ECL1–group 1. **a** Sequence alignment of ECL1 of the cation-selective channel-forming claudins 2 and 15 with the anion-selective channel-forming protein Cldn17. The human sequences are shown corresponding to positions 29–81 in Cldn17 (ECL1 as defined by uniprot. *Green* conserved cysteines, *blue* negatively charged amino acids, *orange* positively charged amino acids, *light orange* histidine. *Boxes* mark the amino acids found to be of opposite charge in cation- and anion-selective claudins (in Cldn17: E44, R45, E48, K65). **b** Transepithelial resistance (TER) of MDCK C7 cells transfected with the generated mutants in comparison with wildtype Cldn17 (wt). Shown are TER values of at least two pooled clones for each mutation. While TER of the empty vector (vec) was doubled compared with that of wt Cldn17, all mutants exhibited no increase in TER, and those with R31E had even more reduced TER values. $*p < 0.05$; $**p < 0.01$ versus wt. **c** Permeability ratio P_{Cl}/P_{Na}. *Ratios above one* represent anion selectivity, while *values below one* represent preference for cations. Except R45A, all mutations caused a loss of anion selectivity of wt Cldn17 and are in a range similar to that of vec, indicating the formation of charge-nonselective channels. $***p < 0.001$. **d** Absolute permeabilities for sodium (*Na*) and the anions—chloride (*Cl*), pyruvate (*Pyr*), nitrate (NO_3), and thiocyanate (*SCN*). $\sim p < 0.05$; $\#p < 0.01$; $+p < 0.001$ versus wt. **e** Representative Western blots of membrane fractions of one clone of the whole cohort of clones for each mutation. Shown is the expression of 3 × FLAG-tagged Cldn17 and the loaded protein represented by β-actin

Table 2 Cldn17 mutations analyzed

Original amino acid	Charge-neutralizing mutant	Charge-reversing mutation
Group 1		
R31		R31E
E44	E44A	
R45	R45A	
E48	E48Q	E48K
Group 2		
K65	K65A	K65E
	K65R	
Group 3		
R56	R56A	
	R56T	
R59	R59A	
R61	R61A	
Group 4		
Y149	Y149A	
H154	H154A	

The previously generated Cldn17 wildtype overexpression clone MDCK C7 Cldn17#10 [11] was used as a positive control in all experiments.

Expression of 3 × Flag-tagged Cldn17 constructs (see subfigures in the respective group's figure) and potential expression changes of other TJ proteins (Supplement Figs. S2 and S3) were verified by immunoblotting and immunofluorescent staining showed correct localization within the TJ, using occludin or ZO-1 as endogenous TJ markers (Supplement Fig. S4). In the following, the analyzed mutations were grouped according to their position in the Cldn17 sequence (Table 2).

Charged residues of group 1 (R31, E44, and E48 but not R45) are involved in Cldn17 channel function

Sequence comparison of ECL1 of the cation-selective claudins 2 and 15 with Cldn17 revealed several positions of opposite or emerging charge, suggesting them to have impact on the charge selectivity of the respective claudin (boxes in Fig. 1a): E44, R45, E48, and K65, the latter being discussed in the next section.

Further on, position R31 was analyzed because its positive charge is highly conserved between claudins indicating that it may be essential in most claudins. We reversed the charge at this position from positive to negative (R31E). The other residues at positions 44 and 45 were mutated to alanine. For position E48, charge-reversing (E48K) and charge-neutralizing (E48Q) substitutions were analyzed.

While transepithelial resistance (TER) for all mutations was reduced compared to the vector control (vec) and similar to wildtype Cldn17 (wt), clones with R31E had even more reduced TER values than the wt (Fig. 1b).

Permeability ratios for chloride over sodium (P_{Cl}/P_{Na}) were calculated from dilution potentials. Since Na^+ and Cl^- are the main well-permeable ions in physiological solutions, P_{Cl}/P_{Na} was used as a measure of charge selectivity. As shown in Fig. 1c, with the exception of R45A, all mutations clearly caused a loss of anion selectivity ($P_{Cl}/P_{NaI} \approx 1$), while P_{Cl}/P_{Na} for wt Cldn17-transfected cells was 1.28 ± 0.03.

More detailed analysis of absolute permeabilities (Fig. 1d) revealed generally higher permeabilities in R31E which did not only comprise chloride (Cl) and sodium (Na) but also larger anions such as pyruvate (pyr), nitrate (NO_3), and thiocyanate (SCN). Because the same charge is present in the cation-selective claudins 2 and 15, this result suggests that R31 might be essential for structural stability of the charge- and size-selective channels formed by these claudins.

For the other positions that affected charge selectivity, the decrease in P_{Cl}/P_{Na} was not due to a reduced P_{Cl}, but to an increased P_{Na}. For all other anions tested, permeabilities were elevated in the mutants of E48, indicating that this position was not only important for charge, but also for size selectivity of Cldn17.

Lysine at position 65 (group 2) is crucial for channel function

As previously shown [11], charge-reversing (K65E) and charge-neutralizing (K65A) mutations were able to abolish the anion selectivity of Cldn17. In order to test whether or not also steric effects play a role, we replaced lysine by arginine (K65R), which maintains the positive charge but differs in size.

While TER (Fig. 2a) in K65E (858 ± 71 Ω cm^2) did not significantly differ from that of wt Cldn17 (700 ± 44 Ω cm^2), TER was increased in K65A (1433 ± 151 Ω cm^2) and even more in K65R (2595 ± 216 Ω cm^2). In all three mutations, anion selectivity was lost in favor of cation selectivity (Fig. 2b). Regarding absolute permeabilities, this was caused by opposite changes of P_{Na} and P_{Cl} which alone did not reach significance, except for K65E where P_{Na} was clearly increased (wt: 0.99 ± 0.07 × 10^{-6} cm/s; K65E: 1.68 ± 0.24 × 10^{-6} cm/s; Fig. 2c). Though at opposite charge selectivity, K65E retained the ion channel property, as TER was close to that of wt Cldn17 (Fig. 2a). K65A exhibited reduced ability for ion channel formation, resulting in absolute permeability values only in the range of the vec. For K65R, the absolute permeabilities were

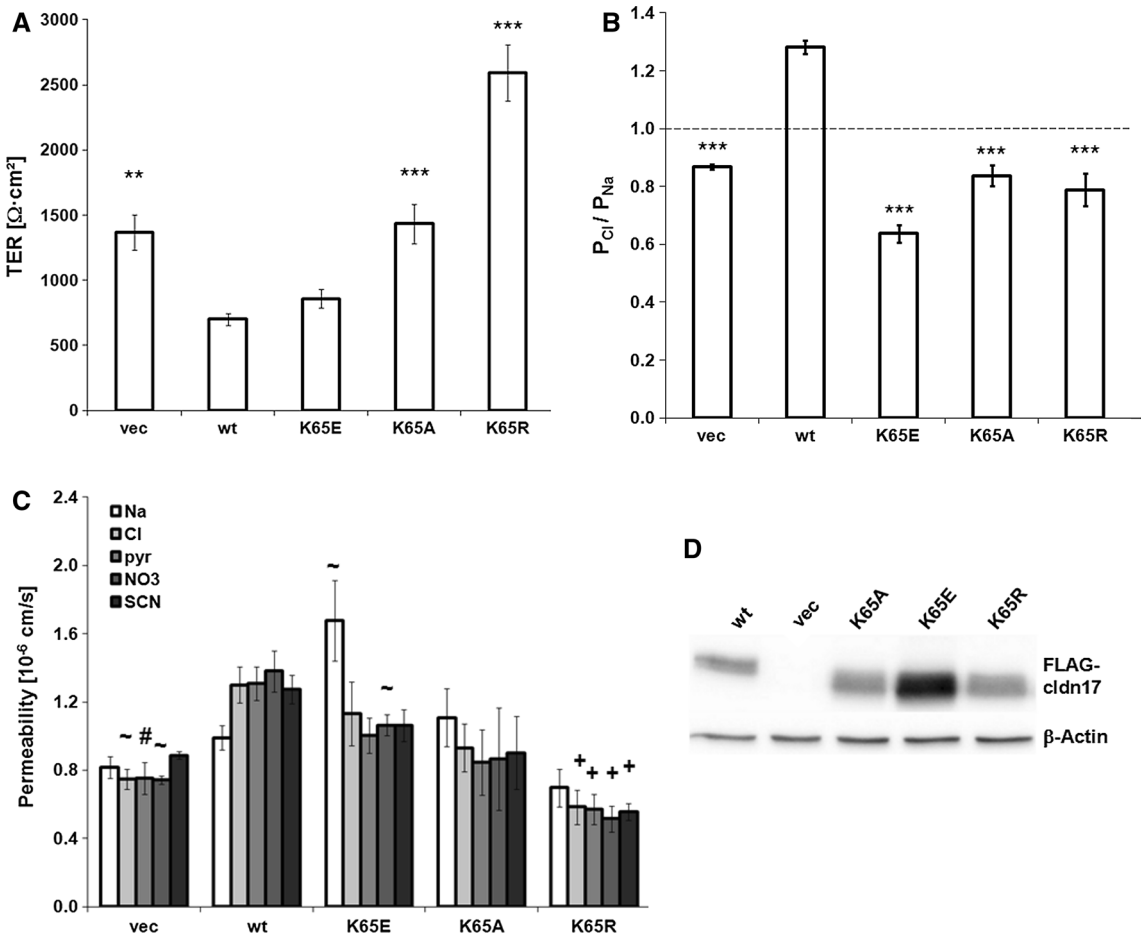

Fig. 2 Mutation of amino acid residues within ECL1–K65. **a** TER of the three mutations of K65 in comparison with wt Cldn17. Shown are TER values of at least two pooled clones of each mutation. Cell layers transfected with the empty vector (vec) and the mutations K65A and K65R produced higher TER than wt. $^{**}p < 0.01$; $^{***}p < 0.001$ versus wt. **b** Permeability ratio P_{Cl}/P_{Na}. *Ratios above one* represent anion selectivity, *values below one* cation selectivity. All three mutations of K65 cause loss of anion selectivity, indicating formation of charge-nonselective channels for K65A and K65R as their ratios are similar to that of vec, while K65E even has a higher preference for cations than vec. $^{***}p < 0.001$ versus wt. **c** Absolute permeabilities for sodium (*Na*) and the anions—chloride (*Cl*), pyruvate (*Pyr*), nitrate (NO_3), and thiocyanate (*SCN*). $\sim p < 0.05$; $\#p < 0.01$; $+p < 0.001$ versus wt. **d** Representative Western blots of membrane fractions of one clone representing the whole group of clones for each mutation. Shown is the expression of 3 × FLAG-tagged Cldn17 and the loaded protein represented by β-actin

even below those of the vec, which was also reflected by the increase of TER (Fig. 2a). Thus, the ability to form a functional channel seems to get lost by introducing the larger amino acid into this position, leading to the conclusion that not only the charge but also stereochemical properties of K65 play a crucial role for formation of an anion-selective channel by Cldn17.

Electron microscopical examination of potential effects of the mutations on the TJ ultrastructure revealed no changes in strand appearance, strand number, TJ meshwork extension, and occurrence of breaks (Supplement Fig. S5). Thus, the mutation-induced changes in channel function are not caused by secondary alterations in TJ ultrastructure.

The positively charged ECL1 residues of group 3 differ between murine and human Cldn17 and have no strong impact on charge selectivity

Sequence analysis of ECL1 of human and mouse Cldn17 showed striking differences at positions 56 to 61. In human Cldn17, this region contains three positively charged arginine residues (R56, R59, and R61) whereas mouse Cldn17 contains no charged amino acids in that region (Fig. 3a).

To investigate a potential influence of this positively charged cluster on channel properties of human Cldn17, the respective amino acids were substituted against an uncharged residue, alanine. For R56 also threonine was introduced to determine the impact of polarity of the side chain.

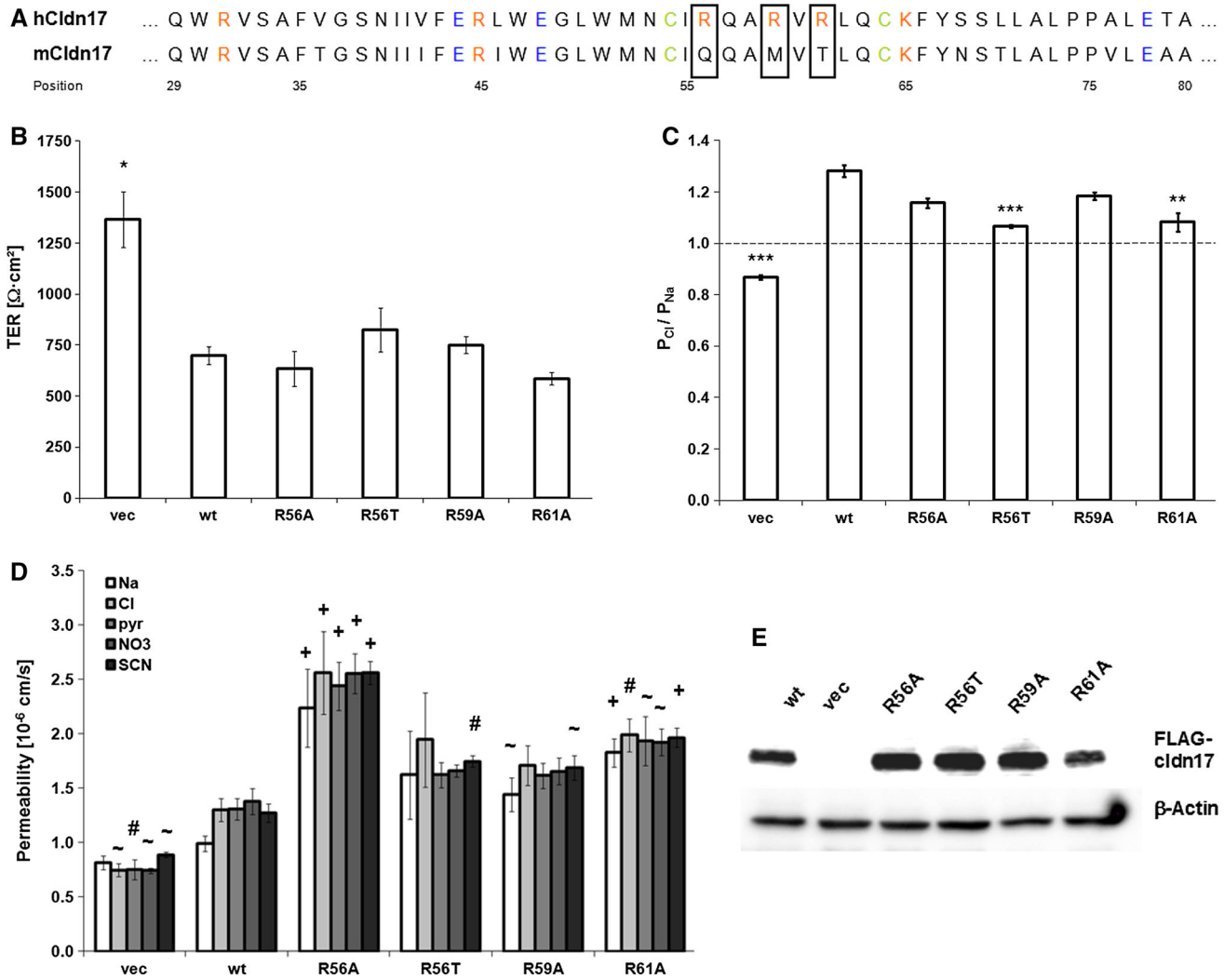

Fig. 3 Mutation of amino acid residues within the ECL1–cluster of charged amino acids between the conserved cysteines. **a** Sequence alignment of ECL1 of murine and human Cldn17. Positions 29–80 which are predicted to form the ECL1 (uniprot) are shown. *Green* conserved cysteines, *blue* negatively charged amino acids, *orange* positively charged amino acids, *light orange* histidine. *Boxes* mark the charged amino acid cluster which is present in human Cldn17, but absent in the murine form (R65, R59, R61). **b** TER of cell layers transfected with the generated mutants in comparison with wt Cldn17. Shown are the TER values of at least two pooled clones of each mutation. None of the mutations led to significant TER changes compared to the wt. $*p < 0.05$ versus wt. **c** Permeability ratio P_{Cl}/P_{Na}. Anion selectivity was maintained in all mutants, though reduced in R56T and R61A. $**p < 0.01$; $***p < 0.001$ versus wt. **d** Absolute permeabilities for sodium (*Na*) and the anions—chloride (*Cl*), pyruvate (*Pyr*), nitrate (NO_3), and thiocyanate (*SCN*). $\sim p < 0.05$; $\#p < 0.01$; $+p < 0.001$ versus wt. **e** Representative Western blots of membrane fractions of one clone representing the whole cohort of clones for each of the four mutations. Shown is the expression of 3 × FLAG-tagged Cldn17 and the loaded protein represented by β-actin

Regarding TER, mutation of these three positions had no significant effects compared to wt Cldn17 (Fig. 3b) and the mutants were still anion selective as indicated by P_{Cl}/P_{Na} ratios above 1 (Fig. 3c). However, anion selectivity of R56T and R61A was lower than that of the wt.

Measurements of absolute permeabilities (Fig. 3d) revealed several changes. Removal of the charged side chain by R56A resulted in elevated permeabilities not only for chloride, but also for sodium and the larger anions—pyruvate, nitrate,and thiocyanate. When the size and polarity of the side chain relative to alanine were increased, these effects were attenuated, and only permeabilities for sodium and thiocyanate were increased. Thus, the charge at R56 appears to be less important for channel properties than the size and polarity. R59A has less impact on permeabilities than R56A as here only permeabilities for thiocyanate, but not for the other ions tested were elevated compared to the wt. R61A showed similar effects as R56A, but to a clearly lesser extent.

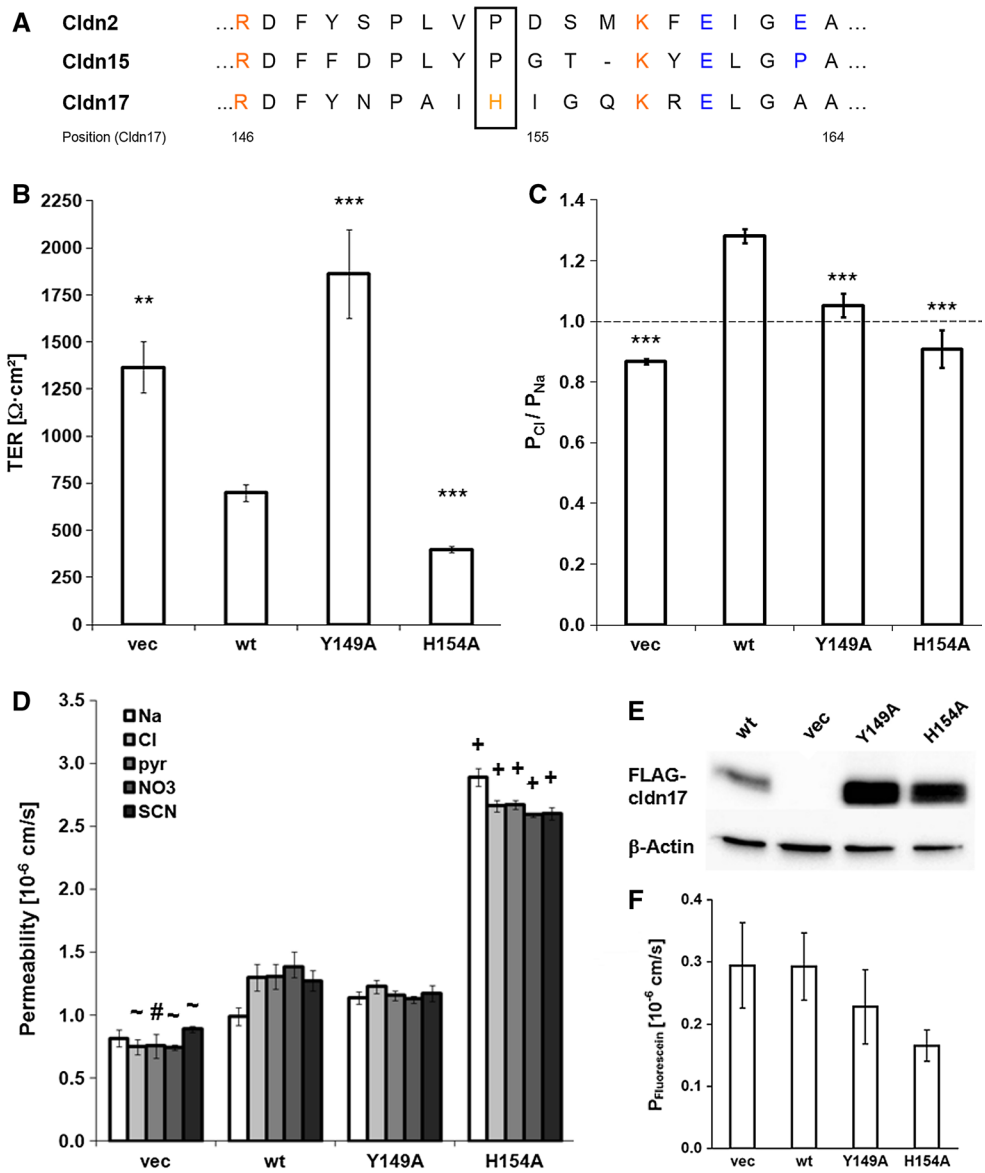

Fig. 4 Mutation of amino acid residues within ECL2. **a** Sequence alignment of ECL2 of the cation-selective channel-forming claudins 2 and 15 with the anion-selective channel-forming protein Cldn17. The human sequences corresponding to positions 146–164 in Cldn17 are shown which are proposed by http://www.uniprot.org to form ECL2. *Blue* negatively charged amino acids, *orange* positively charged amino acids, *light orange* histidine. The *box* marks the prominent difference found (H154) and a position which was mutated because of its exemplary importance for sealing (Y149). **b** TER of the mutants in comparison with wt Cldn17. Shown are the TER values of at least two pooled clones of each mutation. While Y149A leads to an increase, H154 caused a decrease in TER. $^{**}p < 0.01$; $^{***}p < 0.001$ versus wt. **c** Permeability ratio P_{Cl}/P_{Na}. Y149A is as anion selective as wt, while H154A has an increased P_{Cl}/P_{Na} in a range comparable to the vec, suggesting to form a nonselective channel when taking the TER values into account. $^{***}p < 0.001$ versus wt. **d** Absolute permeabilities for sodium (*Na*) and the anions—chloride (*Cl*), pyruvate (*Pyr*), nitrate (NO_3) and thiocyanate (*SCN*). $\sim p < 0.05$; $\#p < 0.01$; $+p < 0.001$ versus wt. **e** Representative Western blots of membrane fractions of one clone representing the whole cohort of clones for each of the mutations. Shown is the expression of the 3 × FLAG-tagged Cldn17 and the loaded protein represented by β-actin. **f** Permeability for fluorescein, a 330 Da anion. Neither wt Cldn17 nor the ECL2 mutants Y149A or H154A had significant influence on fluorescein permeability in comparison to vec

In the ECL2, H154A, but not Y149A, affects the charge selectivity of Cldn17 (group 4)

Comparison of the ECL2 of Cldn2, Cldn15, Cldn17 (Fig. 4a), and other claudins [1] did not reveal the presence of charged residues correlating with a respective ion selectivity. However, an obvious difference in the ECL2 of Cldn17 to other classic claudins is histidine at position 154 (box in Fig. 4a) which is located in the turn region of the loop [1, 34] for 24 out of 28 Cldn17 orthologs (Fig. S1).

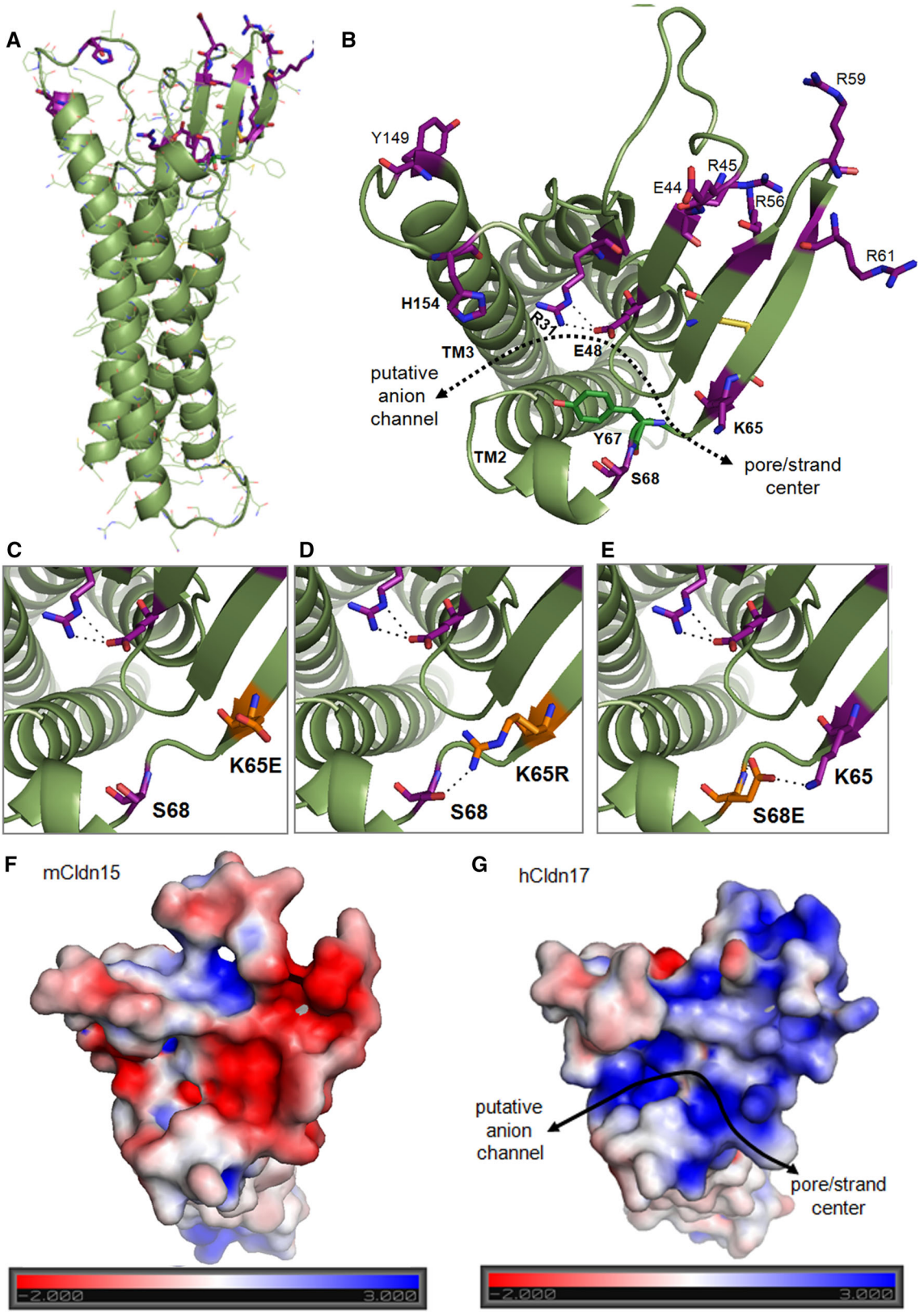
A
B
Y149
R59
R45
E44
R56
R61
H154
R3
E48
TM3
putative
anion
channel
K65
Y67
TM2
S68
pore/strand
center
C
K65E
S68
D
K65R
S68
E
K65
S68E
F
mCldn15
−2.000
3.000
G
hCldn17
putative
anion
channel
pore/strand
center
−2.000
3.000

◀**Fig. 5** Structural features of the Cldn17 protomer involved in anion channel formation. **a** Homology model of hCldn17 based on mCldn15 template (PDB 4P79), *side view* (parallel to the cell membrane) with backbone as cartoon, residues mutated in this study as sticks in *magenta*, other residues as *lines*, O atoms *red*, N atoms *blue*. **b** *Top view* (from the extracellular side) of the protomer highlighting the proposed part (*dotted double arrow*) of the oligomeric anion channel. One opening of the pore is proposed to be located between the extracellular ends of TM2 and TM3. H154 in the ECL2 might be involved in the formation of an opening that attracts anions. R31 and E48 are part of an electrostatic network (*dotted lines*) proposed to line the pore along with Y67 (*green stick*). K65 is responsible for anion selectivity and likely positioned at the proposed second pore opening between end of β4-strand and S68 close to the small α-helix. This protomer opening might be at the center of the oligomeric pore within the TJ strand (Fig. 7). E44, R45, R56, R59, and R61 are positioned at the opposite end of the β-sheet. Y149 is implicated in intermolecular strand formation. The C54–C64 bridge in ECL1 is shown in yellow. **c** K65E (*orange*) preserves the distance to S68 but not the capability for electrostatic interaction with anions, consistent with loss of anion selectivity. **d** K65R (*orange*) might result in a H-bond (*dotted line*) with S68, causing blockade of the pore. **e** S68E (*orange*) might result in electrostatic interaction (*dotted line*) with K65, causing blockade of the pore. Differing electrostatic potentials (units *kT/e*) on the surface of **f** mCldn15 and **g** hCldn17 protomer in the area of the proposed ion channel (*double arrow*) are in line with the opposite charge selectivity of Cldn15 and Cldn17, respectively

Histidine's imidazole side chain, because of its pKa of 6.0, can function as an electron acceptor as well as electron donor under physiological conditions. As residues with such properties are absent in Cldn2 as well as in Cldn15, the significance of H154 was analyzed.

H154A resulted in reduced TER compared to wt values (Fig. 4b) and these clones clearly lost anion selectivity (P_{Cl}/P_{Na} 0.91 ± 0.07) (Fig. 4c). These changes were based on a strong increase of permeabilities for sodium and all tested anions. These observations suggested H154 being not only involved in charge selectivity but also in size selectivity.

Since the Cldn5 ECL2 residues R145, Y148, Y158, and E159 were found to participate in the general sealing properties of that claudin [16], exemplarily also position Y149 (corresponding to Y148 of Cldn5 and containing a aromatic residue conserved between classic claudins and species) was studied to get insight into the general concept of pore formation (Fig. 4a). Y149A led to a TER increase indicating reduction of overall ion permeability. This is reflected by a reduced P_{Cl}/P_{Na} ratio (Fig. 4c) and a tendency (below significance) to decreased permeabilities compared to wt (Fig. 4d). The contribution of the two ECL2 residues to size selectivity was determined from the permeability of the paracellular marker fluorescein (330 Da), which is also an anion. It remained unaffected for Y149A as well as for H154A (Fig. 4f) indicating that these positions within the ECL2 have no significant influence on the passage of larger molecules.

Since ECL2, in particular the residue corresponding to Y149 of Cldn17, was suggested to be involved in intermolecular claudin interaction [17, 19], we also analyzed the ability of Cldn17wt, Cldn17-Y149A, and Cldn17-H154A for *trans*-interaction. CFP-labeled Cldn17 constructs were expressed in the TJ-devoid cell line HEK293 and the claudin enrichment at cell–cell contacts was analyzed and served as a measure of *trans*-interaction [17]. Cldn17-Y149A and Cldn17-H154A showed clear enrichment at contacts between neighboring claudin-expressing cells similar to Cldn17-wt. This result indicates that a mutation of Y149 or H154 does not prevent the capability of Cldn17 for *trans*-interaction (Fig. S6).

In conclusion, the data suggest that both Y149 and H154 are involved in constitution of the Cldn17 anion channel in different ways.

Structural features of Cldn17 contributing to anion channel formation

To gain structural insight into the anion channel formed by Cldn17 and to explain the experimental findings, homology modeling of human Cldn17 was performed. The recently released crystal structure of the cation channel-forming murine Cldn15 was used as template (PDB: 4P79; [19]) because the sequence similarity between Cldn15 and Cldn17 in the part where the structure was resolved is high (51 %). A homology model was generated and the residues mutated in the present study were mapped on the model (Fig. 5a, b). The model shows that three residues with strong functional relevance (R31, E48, K65) are located on one side of the β-sheet in the ECL1 close to the membrane.

E44 points in a similar direction but is located at the other end of the β-sheet. Several arginines (R45, R56, R59, R61) cluster at one corner of the β-sheet and point rather to other directions than R31, E44, E48, and K65. Y149 is part of a conserved hydrophobic pit in the ECL2 and found to be involved in strand formation [17, 19]. H154 points to the opposite side in the turn region of the ECL2. After a crystal structure of mouse Cldn19 (63 % sequence similarity to Cldn17) was released recently (PDB: 3X29; [20]), an additional homology model was generated based on this Cldn19 template. In both models, the residues mutated in this study were positioned in a similar manner supporting the validity of the models (Fig. S7).

S68 is involved in anion selectivity

Modeling of the Cldn17 anion channel indicated S68 to be involved in the formation of the channel. We hypothesize that lack of interaction between S68 and K65 might enable ions to pass from one to a neighboring protomer (Fig. 5b).

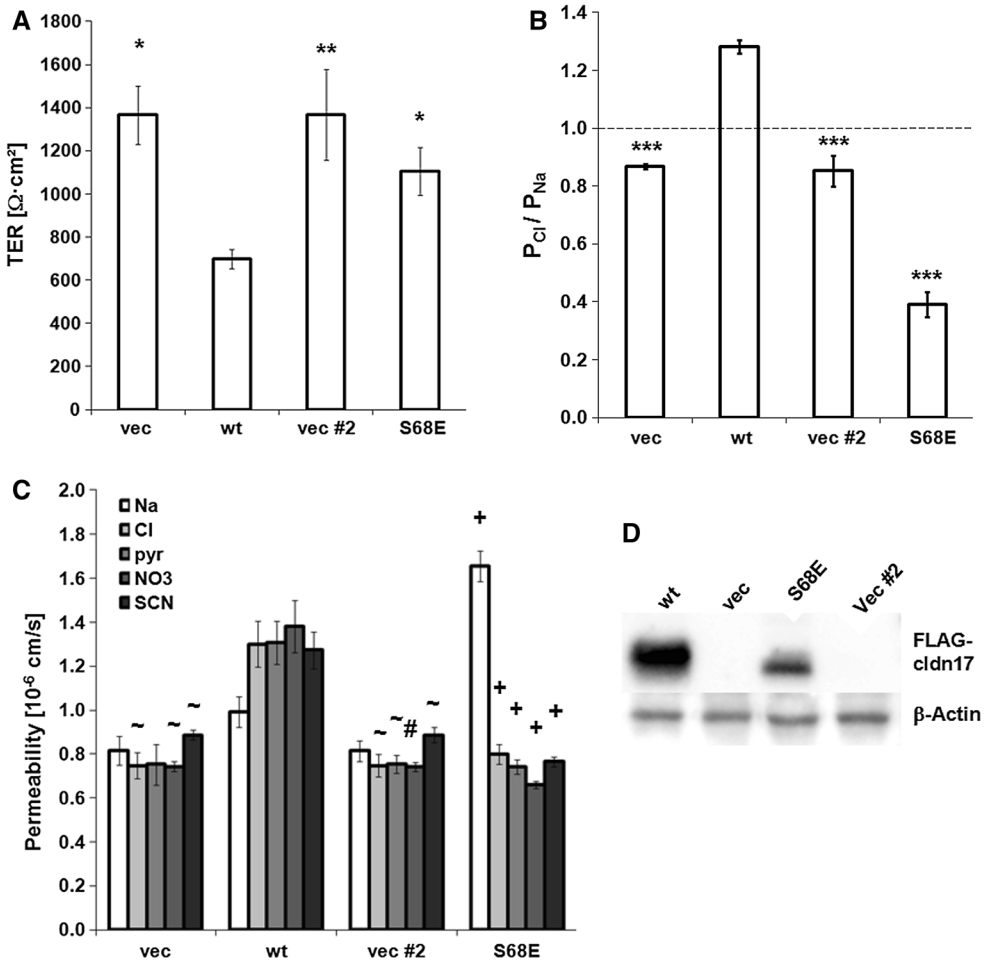

Fig. 6 Mutation of S68. **a** TER of the generated mutants in comparison with wt Cldn17. Shown are the TER values of at least two pooled clones of each mutation. As the S68E mutation was generated independently of all other transfections, a second vec (vec#2) was generated in parallel and used for confirmation of old and new clones by direct comparison with the first vec. S68E lead to increase of TER compared to wt Cldn17. $*p < 0.05$; $**p < 0.01$; $***p < 0.001$ versus wt. **b** Permeability ratio P_{Cl}/P_{Na}. *Ratios above one* represent anion selectivity, *values below one* cation selectivity. S68E exhibited low P_{Cl}/P_{Na} compared to wt and even to vec, indicating a high preference for cations. $***p < 0.001$ versus wt. **d** Absolute permeabilities for sodium (*Na*) and the anions—chloride (*Cl*), pyruvate (*Pyr*), nitrate (NO_3), and thiocyanate (*SCN*). While decreased permeabilities for anions were obtained in S68E, permeability for sodium was increased. $\sim p < 0.05$; $\#p < 0.01$; $+p < 0.001$ versus wt. **e** Representative Western blots of membrane fractions of one clone representing the whole cohort of clones. Shown is the expression of 3 × FLAG-tagged Cldn17 and the loaded protein represented by β-actin

The side chain of K65 might be too short for an H-bond with that of S68. K65R, but not K64E, introduces a longer side chain capable of forming an H-bond with S68 which could explain the hindrance of pore formation by K65R (Fig. 5c, d). To test that hypothesis, a residue with a long and negatively charged side chain potentially capable of interacting with K65 was introduced by S68E substitution (Fig. 5e).

Indeed, for $Cldn17_{S68E}$, TER was higher than for $Cldn17_{wt}$ and was not significantly different from vector controls (Fig. 6a). The ratio P_{Cl}/P_{Na} of 0.39 ± 0.05 indicated a clear change from anion to cation selectivity (Fig. 6b), indicating a hindrance of the anion channel function. Evaluation of absolute permeabilities revealed for all anions tested a tightening effect of S68E in range of the vector controls, while permeability for sodium was increased (Fig. 6c). Thus, our data indicate that S68E inhibits anion permeability by reversing the charge selectivity of the remaining and partially functional channel formed by $Cldn17_{S68E}$. These results support the hypothesis that lack of interaction between S68 and K65 contributes to pore formation.

Discussion

Functional analysis of Cldn17 mutants reveals residues involved in anion channel formation

Cldn17 was previously identified as forming anion-selective paracellular channels [11] but little is known so far about the molecular properties allowing for that selectivity. Charged residues located one or two positions C-terminally of the strongly conserved cysteines in ECL1 (C64 in Cldn17) were already studied in several claudins (Cldn2 [14]; Cldn4 [26, 27]; Cldn10a [8]; Cldn15 [27]. For Cldn17 the presence of K65 was demonstrated to be crucial for anion selectivity [11].

Comparing the ECL1 of Cldn2 and Cldn15 with that of Cldn17 by sequence alignment revealed several further residues potentially being involved in differentiation between cations and anions and the formation of the ion-selective channels.

Besides K65, we were able to show that E44, E48, and R31 are influencing the formation of the anionic charge selectivity of Cldn17. In contrast, no clear indication was found for participation of a positively charged cluster (R56, R59, and R61) in charge selectivity. Consistent with this finding, these residues are not conserved between human and murine Cldn17. However, the positively charged cluster is part of a region between the two conserved cysteines (Fig. 5b) which has been shown to contribute to charge selectivity in other claudins [27, 28]. The charge-reversing mutation at position 55 (D55R) largely affected Cldn15, converting it from cation to anion selectivity [27], and in Cldn19 Q57E has been shown to cause familial hypomagnesaemia with hypercalciuria and nephrocalcinosis (FHHNC; [28]). On the other hand, mutation of H57 in Cldn2 did not alter ion permeation across the cation channel although this residue was modeled inside the Cldn2 pore [13]. For Cldn17, side chain substitutions of the arginines in this region had no clear effect, indicating that there seems to be no obvious pattern between different claudin species. Therefore, it has to be individually assessed whether or not a given charged residue is involved in claudin channel formation.

While for the ECL1 involvement in charge selectivity has been proposed [1, 29], impact of the ECL2 often has been neglected: Alexandre et al. used site-directed mutagenesis to analyze positions D147 and E160 of Cldn7 and found no changes in permeability properties compared to wt Cldn7 [30]. In Cldn16, point mutations in ECL2 are found in patients with FHHNC. However, overexpression of these Cldn16 mutants in LLC-PK1 or MDCK C7 cells often lead to dislocation into the endoplasmatic reticulum [31, 32]. As mentioned before, ECL2 mutations of Cldn5 affect TER as well as the passage of small and large molecules [16].

In Cldn17, we showed a clear participation of the ECL2 residue H154 in anion permeability. A histidine side chain (pKa of 6.0) is able to donate and also accept electrons under physiological conditions. It might either directly support the passage of anions through the channel formed by Cldn17 or participate in the interaction of two Cldn17 protomers forming the channel. For Cldn5, it was shown that ECL2 mutations inhibited intermolecular interaction and affected barrier properties [16].

Homology modeling indicates a furrow within the Cldn17 protomer to line the anion channel

According to homology modeling, Cldn17 (Figs. 5a, S7) shows a folding very similar to that of Cldn15 [19], Cldn19 [20], and other classic claudins [33, 34] including a left-handed four-transmembrane helix bundle and an extracellular β-sheet. However, there are slight differences within the helix bundle, the transition between the β1-strand in ECL1 and β5-strand in the ECL2, the small helix in the ECL1 and the turn region of the ECL2.

The residues mutated in the study were mapped in the models (Figs. 5a, b, S7). Interestingly, substitution of K65, corresponding to the charge selectivity filter in Cldn2, had in general a stronger effect on TER, ion permeability, and charge selectivity than the substitution of other positive charges in the ECL1 (R45, R56, R59, R61). This finding indicated K65 to be involved more intensely in charge-selective ion permeation than the other positively charged residues clustered at the opposite side of the β-sheet.

$Cldn17_{K65E}$ formed an ion-permeable but rather cation-selective channel. In contrast, K65R substitution preserving the positive charge resulted in loss of ion permeability.

Charge removal and size reduction by K65A blocked the formation of a distinct charge-selective channel. These findings indicate that in addition to the positive charge, the size, the shape, and a particular H-bonding capability of K65 are necessary for the formation of an anion-selective ion channel.

Modeling indicated that in contrast to the side chains of K65, A65, or E65, the longer side chain of R65 may be able to form an H-bond with S68 (Fig. 5b–e). Such a direct interaction might block the ion passage. Consistent with this idea, similar "blocking" electrostatic interactions ("closed path") would be possible also for barrier-forming claudins (Cldn1, -2 to -9, -19) with participation of Lys at the position corresponding to K65 in Cldn17 and aspartate (Asp) at the position corresponding to S68 in Cldn17 [1]. In the crystal structure of Cldn19 (PDB: 3X29; [20]), the side

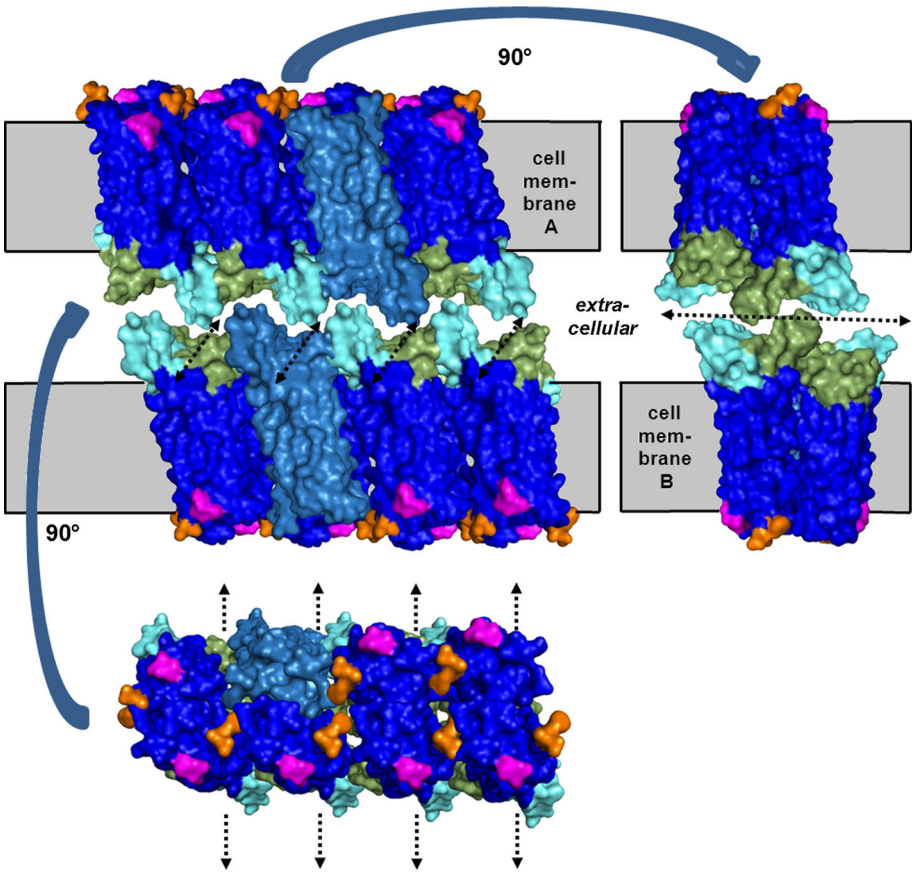

Fig. 7 Basic schema of tentative architecture of the oligomeric pore within the polymeric TJ strand, *side view* (*top left*), *front view* (*right*), and *top view* (*bottom*). The schema is a modification of an antiparallel double row model of Cldn15 TJ strands [25] with antiparallel *cis*-arrangement of two linear *cis*-polymers of claudin protomers. Protomer surfaces are shown either in sky blue or for different regions in *blue* (TMs), *green* (ECL1), *cyan* ECL2, *orange* (TM1 end), or *magenta* (TM4 end). TJ strands are formed by *trans*-interaction between the extracellular domains and *cis*-interactions within the double rows. Direction of ion permeation through the strands is indicated by *dotted arrows*. The *white gaps* in the extracellular space indicate that the *trans*-interfaces are unclear. In contrast to the model suggested by Suzuki et al., in this schema, the protomers are arranged with potential transmembranal contacts as experimentally indicated [2, 36, 38]. The schema is based on the claudin-15 protomer structure (PDB: 4P79, [19]), while intermolecular interfaces were not precisely modeled or docked

chains of K65 and D68 were not resolved. Nevertheless, the distance between the corresponding Cα-atoms would enable intramolecular interaction of the side chains. In contrast, other channel-forming claudins (Cldn2, -10a, -10b, -15) lack residues which electrostatically and sterically fit to each other at the corresponding positions ("open path").

This "open or closed path" hypothesis is further supported by the finding that S68E, which should enable electrostatic intramolecular interaction with K65, strongly inhibited the anion channel formation (Fig. 6). However, it neither can be excluded that a "closed path" is a result of intermolecular interaction between positions corresponding to 65 and 68 in Cldn17, nor can it be excluded that K65 and S68 contribute by other interactions or in another way to the open pore.

For Cldn17, 20 out of 28 orthologs contain a Ser or Thr at position 68 (Fig. S1). A longer Asn or Asp at position 68 is present in five and three orthologs, respectively. These longer hydrophilic side chains might enable interaction with K65. However, Asn/Asp at position 68 coincides with charge differences in the region of the arginine cluster (R56-R61), (Fig. S1). This coincidence might indicate a potential intermolecular interaction between the region around position 68 and the region 56-61. Whether these sequence differences between species affect the ion permeability of Cldn17 channels is so far unclear.

Additionally, S68E substitution reversed the charge selectivity of the remaining and still partially functional ion channel. The observed increase of permeability for sodium could be due to attraction of positive charges by E68. In any case, the data show that position 68 of Cldn17 is involved in the formation of an anion-selective channel.

In summary, we suggest for Cldn17 the ions to pass the gap between K65 and S68. For other channel-forming claudins, the ions could potentially also pass a

corresponding gap. An alternative route for ions passing residues N-terminal of K65 on the β4 strand is not supported by our data. The ions might reach K65 from a hydrophilic furrow spanning from a gap between the extracellular ends of TM2 and TM3 along R31, E48, and N53 to K65/S68 (Fig. 5b, g, double arrows). This putative course of the anion channel is supported by the following experimental findings:

1. H154A in the turn region of the ECL2 inhibits anion selectivity but not *trans*-interaction. The ECL2 of most other classic claudins has been shown to contain a small hydrophobic residue at the corresponding position [17, 33–36]. The steric and hydrophilic features of H154 in Cldn17 thus might be involved in the formation of an opening which attracts anions.
2. R31E, E48K, and E48Q inhibit anion selectivity of the channel. R31E could directly inhibit attraction of anions. Furthermore, R31 and E48 are part of a network of electrostatic interactions reaching from TM3 to the β4 strand. Electrostatic networks between the corresponding positions likely exist also in other classic claudins. In the channel-forming claudins, these residues could be involved in electrostatic attraction of hydrated or partly dehydrated ions. In Cldn17, R31E as well as E48K and partially also E48Q would block the electrostatic interaction between R31 and E48. The latter is formed in the Cldn17 model (Fig. 5) and between the corresponding R30 and E46 in the Cldn15 structure (PDB 4P79). This loss of interaction could inhibit routing of the ions or disturb the pore formation for structural reasons. Y67 in Cldn2 and F66 in Cldn10b were reported to line the respective cation channel [3]. Similarly and consistent with the proposed furrow to line the pore, Y67 in Cldn17 is located between R31/E48 and K65/S68 (Fig. 5b).
   Also the differing electrostatic potentials between mCldn15 and hCldn17 (Fig. 5f, g) in the area of the proposed furrow are in line with the opposite charge selectivity of Cldn15 and Cldn17, respectively.
3. $Cldn17_{Y149A}$ is still capable of homophilic *trans*-interaction; nevertheless it does not form a wild type-like ion channel. The corresponding Y148 in Cldn5 and Y147 in Cldn3 have been shown to be directly or indirectly involved in strand formation [17, 37] In Cldn15, the corresponding F147 forms a pit together with F146, L158, and E159 which has been reported to be involved in a *cis*-interaction observed in the crystal. Therefore, Y149A in Cldn17 might influence intermolecular interaction within the heteropolymeric strand leading to a structural change inhibiting formation of the oligomeric pore. Within a channel-forming oligomer E44 and synergistically, the arginine cluster (R45, R56, R59, R61) could still contribute to the pore lining.

In conclusion, we propose the above-described furrow (Fig. 5) in the center of the extracellular part of the Cldn17 protomer to line the anion pore which is likely to be formed by a claudin oligomer in which (1) *trans*-interaction closes the pore to the top and (2) *cis*-interactions between more than two protomers elongate the channel and together with *trans*-interaction result in polymerization perpendicular to the channel (Fig. 7). Further structure–function studies are needed to characterize the interaction interfaces between the protomers within the claudin polymer.

For the claudin protomer, we identified structural determinants in ECL1 and ECL2 which are involved in formation and charge selectivity of the Cldn17-based paracellular anion channel.

Acknowledgments We appreciate the excellent technical assistance of In-Fah M. Lee and Detlef Sorgenfrei. This study was supported by grants of the Deutsche Forschungsgemeinschaft (DFG FOR 721).

Compliance with ethical standards

Conflict of interest The authors declare no conflicts of interest.

References

1. Krause G et al (2008) Structure and function of claudins. Biochim Biophys Acta 1778(3):631–645
2. Colegio OR et al (2003) Claudin extracellular domains determine paracellular charge selectivity and resistance but not tight junction fibril architecture. Am J Physiol Cell Physiol 284(6):C1346–C1354
3. Li J et al (2013) Conserved aromatic residue confers cation selectivity in claudin-2 and claudin-10b. J Biol Chem 288(31):22790–22797
4. Günzel D, Fromm M (2012) Claudins and other tight junction proteins. Compr Physiol 2(3):1819–1852
5. Mineta K et al (2011) Predicted expansion of the claudin multigene family. FEBS Lett 585(4):606–612
6. Krug SM, Schulzke JD, Fromm M (2014) Tight junction, selective permeability, and related diseases. Semin Cell Dev Biol 36:166–176
7. Amasheh S et al (2002) Claudin-2 expression induces cation-selective channels in tight junctions of epithelial cells. J Cell Sci 115(Pt 24):4969–4976
8. Van Itallie CM et al (2006) Two splice variants of claudin-10 in the kidney create paracellular pores with different ion selectivities. Am J Physiol Renal Physiol 291(6):F1288–F1299
9. Günzel D et al (2009) Claudin-10 exists in six alternatively spliced isoforms that exhibit distinct localization and function. J Cell Sci 122(Pt 10):1507–1517
10. Van Itallie CM, Fanning AS, Anderson JM (2003) Reversal of charge selectivity in cation or anion-selective epithelial lines by expression of different claudins. Am J Physiol Renal Physiol 285(6):F1078–F1084
11. Krug SM et al (2012) Claudin-17 forms tight junction channels with distinct anion selectivity. Cell Mol Life Sci 69(16):2765–2778

12. Rosenthal R et al (2010) Claudin-2, a component of the tight junction, forms a paracellular water channel. J Cell Sci 123(Pt 11):1913–1921
13. Angelow S, Yu AS (2009) Structure-function studies of claudin extracellular domains by cysteine-scanning mutagenesis. J Biol Chem 284(42):29205–29217
14. Yu AS et al (2009) Molecular basis for cation selectivity in claudin-2-based paracellular pores: identification of an electrostatic interaction site. J Gen Physiol 133(1):111–127
15. Wen H et al (2004) Selective decrease in paracellular conductance of tight junctions: role of the first extracellular domain of claudin-5. Mol Cell Biol 24(19):8408–8417
16. Piehl C et al (2010) Participation of the second extracellular loop of claudin-5 in paracellular tightening against ions, small and large molecules. Cell Mol Life Sci 67(12):2131–2140
17. Piontek J et al (2008) Formation of tight junction: determinants of homophilic interaction between classic claudins. FASEB J 22(1):146–158
18. Veshnyakova A et al (2012) Determinants contributing to claudin ion channel formation. Ann N Y Acad Sci 1257:45–53
19. Suzuki H et al (2014) Crystal structure of a claudin provides insight into the architecture of tight junctions. Science 344(6181):304–307
20. Saitoh Y et al (2015) Structural insight into tight junction disassembly by Clostridium perfringens enterotoxin. Science 347(6223):775–778
21. Biasini M et al (2014) SWISS-MODEL: modelling protein tertiary and quaternary structure using evolutionary information. Nucleic Acids Res 42((Web server issue)):W252–W258
22. Bordoli L et al (2009) Protein structure homology modeling using SWISS-MODEL workspace. Nat Protoc 4(1):1–13
23. Arnold K et al (2006) The SWISS-MODEL workspace: a web-based environment for protein structure homology modelling. Bioinformatics 22(2):195–201
24. Benkert P, Kunzli M, Schwede T (2009) QMEAN server for protein model quality estimation. Nucleic Acids Res 37((Web Server issue)):W510–W514
25. Suzuki et al (2015) Model for the architecture of claudin-based paracellular ion channels through tight junctions. J Mol Biol 427(2):291–297
26. Hou J et al (2010) Claudin-4 forms paracellular chloride channel in the kidney and requires claudin-8 for tight junction localization. Proc Natl Acad Sci USA 107(42):18010–18015
27. Colegio OR et al (2002) Claudins create charge-selective channels in the paracellular pathway between epithelial cells. Am J Physiol Cell Physiol 283(1):C142–C147
28. Konrad M et al (2006) Mutations in the tight-junction gene claudin 19 (CLDN19) are associated with renal magnesium wasting, renal failure, and severe ocular involvement. Am J Hum Genet 79(5):949–957
29. Krause G, Protze J, Piontek J (2015) Assembly and function of claudins: Structure-function relationships based on homology models and crystal structures. Semin Cell Dev Biol. doi:10.1016/j.semcdb.2015.04.010 [Epub ahead of print]
30. Alexandre MD et al (2007) The first extracellular domain of claudin-7 affects paracellular Cl- permeability. Biochem Biophys Res Commun 357(1):87–91
31. Hou J, Paul DL, Goodenough DA (2005) Paracellin-1 and the modulation of ion selectivity of tight junctions. J Cell Sci 118(Pt 21):5109–5118
32. Kausalya PJ et al (2006) Disease-associated mutations affect intracellular traffic and paracellular Mg^{2+} transport function of Claudin-16. J Clin Invest 116(4):878–891
33. Rossa J et al (2014) Molecular and structural transmembrane determinants critical for embedding claudin-5 into tight junctions reveal a distinct four-helix bundle arrangement. Biochem J 464(1):49–60
34. Protze J et al (2015) Directed structural modification of Clostridium perfringens enterotoxin to enhance binding to claudin-5. Cell Mol Life Sci 72(7):1417–1432
35. Winkler L et al (2009) Molecular determinants of the interaction between *Clostridium perfringens* enterotoxin fragments and claudin-3. J Biol Chem 284(28):18863–18872
36. Rossa J et al (2014) Claudin-3 and claudin-5 protein folding and assembly into the tight junction are controlled by non-conserved residues in the transmembrane 3 (TM3) and extracellular loop 2 (ECL2) segments. J Biol Chem 289(11):7641–7653
37. Piontek J et al (2011) Elucidating the principles of the molecular organization of heteropolymeric tight junction strands. Cell Mol Life Sci 68(23):3903–3918
38. Van Itallie CM, Mitic LL, Anderson JM (2011) Claudin-2 forms homodimers and is a component of a high molecular weight protein complex. J Biol Chem 286(5):3442–3450